Article

Mechano-Sensitive Synthetic Ion Channels

Takahiro Muraoka, Kaori Umetsu, Kazuhito V. Tabata, Tsutomu Hamada, Hiroyuki Noji, Takashi Yamashita, and Kazushi Kinbara

J. Am. Chem. Soc., **Just Accepted Manuscript** • DOI: 10.1021/jacs.7b09515 • Publication Date (Web): 27 Oct 2017

Mechano-Sensitive Synthetic Ion Channels

Takahiro Muraoka,*[,†,‡] Kaori Umetsu,[§] Kazuhito V. Tabata,[¶] Tsutomu Hamada,[⊥] Hiroyuki Noji,[¶] Takashi Yamashita[#] and Kazushi Kinbara*[,†,§]

[†]School of Life Science and Technology, Tokyo Institute of Technology, 4259 Nagatsuta-cho, Midori-ku, Yokohama 226-8503, Japan.

[‡]Precursory Research for Embryonic Science and Technology, Japan Science and Technology Agency, 4-1-8 Honcho, Kawaguchi, Saitama 332-0012, Japan.

[§]Institute of Multidisciplinary Research for Advanced Materials, Tohoku University, 2-1-1, Katahira, Aoba-ku, Sendai 980-8577, Japan.

[¶]Department of Applied Chemistry, School of Engineering, The University of Tokyo, Bunkyo-ku, Tokyo 113-8656, Japan.

[⊥]School of Materials Science, Japan Advanced Institute of Science and Technology, 1-1 Asahidai, Nomi, Ishikawa 923-1292, Japan.

[#]Department of Pure and Applied Chemistry, Tokyo University of Science, 2641 Yamazaki, Noda-shi, Chiba 278-8510, Japan.

ABSTRACT: Mechanical stress is a ubiquitous stimulus sensed by membrane proteins, but rarely by synthetic molecules. Inspired by mechano-sensitive ion channels found in cell membranes, tension-responsive transmembrane multi-block amphiphiles were developed. In membranes, a single-transmembrane amphiphile responded to both expanding and contracting tensions to weaken and strengthen the stacking of membrane-spanning units, respectively, and ion transportation is triggered by expanding tension to form a supramolecular channel, while little transportation is observed under a tensionless condition. In contrast, a three-transmembrane amphiphile showed little spectroscopic response to tensions likely due to weaker stacking of membrane-spanning units than the single-transmembrane amphiphile. Nevertheless, the three-transmembrane amphiphile shows ion transportation by forming a unimolecular channel even under a tensionless condition, and the ion transporting activity decreased by expanding tension. Interestingly, the estimated operating force of these synthetic systems was comparable to that of the mechano-sensitive proteins. This study opens the door toward new mechano-sensitive molecular devices.

INTRODUCTION

Mechanochemistry gains increasing attention at the interface between chemistry and mechanical engineering. Not only detection of shear forces for bond cleavages but also induction of chemical reactions, non-covalent bond formation, and phase transitions have actively been demonstrated.[1–17] These examples have mostly been realized by polymers, liquid crystals, and organic/inorganic crystalline materials, where the macroscopic forces are applied to the bulk substances. Meanwhile, in the biological systems, microscopic mechanical forces produced by sound, gravity or osmotic pressure are sensed by membrane proteins in a cytoplasmic membrane such as mechano-sensitive channels (MSCs). MSCs respond to the changes in the membrane tension so as to function as safety valves against the osmotic shock in bacteria, and also as sensors for touch and sound waves in higher organisms.[18] The membrane tension triggers conformational changes of MSCs to open the channel and flow ions or small signaling molecules, which releases osmotic stress and activates signaling cascades. Inspired by such mechano-sensitive proteins, Matile and coworkers developed supramolecular systems probing a transition between liquid-ordered and solid-ordered membrane phases, where changes in the physical properties such as viscosity and elastic modulus could be visualized by fluorescence signals.[19–23] A conformational change and control of guest recognition by synthetic molecules were demonstrated at the air–water interface using Langmuir monolayer.[24–28] However, the original functions of MSCs, *i.e.*, the control of substance-transportation through a membrane by mechanical stimuli, remains a significant challenge in development of smart biomimetic molecular devices. Herein, we demonstrate a mechano-sensitive ion transportation switch by synthetic transmembrane molecules, which respond to both expanding and contracting tensions applied to the membrane.

In recent years, we have been developing synthetic mimics of multipass transmembrane (MTM) proteins, consisting of repeating oligo(ethylene glycol) chains and aromatic units.[29–33] We found that the aromatic units of the MTM mimics tend to self-assemble through intra- and intermolecular interactions in the lipid bilayer, which leads to formation of supramolecular ion channels. These facts, coupled with the precedent examples of luminescent tension-sensing molecules,[34] inspired us to realize that the intra- and intermolecular aromatic stacking of MTM mimics would possibly be responsive to the change in the membrane tension, thereby influencing the transportation activity. In order to acquire the sensitivity to the membrane tension, moderately destabilized aromatic stacking is likely advantageous, which could be attained by substituents on the aromatic units causing steric hindrance among the π-π assembling moieties. On the basis of these backgrounds, we designed synthetic MTM mimics **1** and **2** in this study, which have a multi-block structure including alternating hydrophilic

and hydrophobic units. Indeed, octaethylene glycol (OEG) chains and 3,3'-dimethyl-5,5'-bis(phenylethynyl)-2,2'-bipyridine (BPBP) units were introduced as the hydrophilic and hydrophobic units, respectively, where the BPBP units are expected to span the hydrophobic layer of the lipid bilayer. Since fluorescence emission provides important information regarding the conformation and assembly of the hydrophobic parts, bipyridyl units, having higher fluorescence quantum yield than biphenyl, were introduced in the core.[35] In addition, methyl groups were introduced at the 2- and 2'-positions of the BPBP units to generate a steric hindrance. We found that **1** and **2** (Figure 1) respond to the membrane tension by changing the stacking mode of the BPBP so as to influence on the ion transportation efficiency.

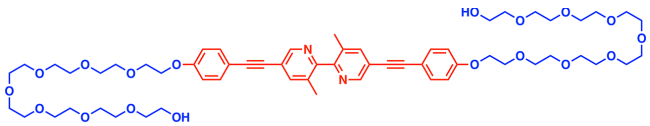

1

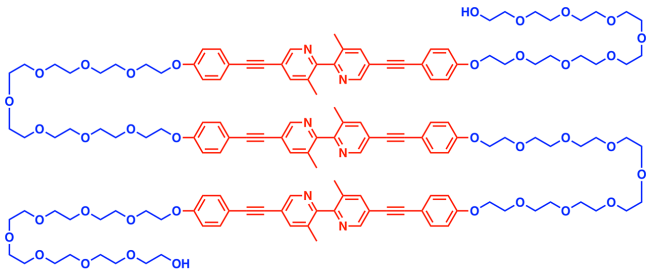

2

Figure 1. Molecular structures of multi-block amphiphiles **1** and **2**.

RESULTS AND DISCUSSION

Self-Assembly of MTM Mimics in Aqueous Media.

1 was synthesized by the coupling reaction between 5,5'-diethynyl-3,3'-dimethyl-2,2'-bipyridine and 23-(4-iodophenoxy)-3,6,9,12,15,18,21-heptaoxatricosan-1-ol, and this scheme was also extended to the synthesis of **2** (see Supporting Information). Since **1** and **2** are amphiphilic, we first investigated the self-assembling behaviors of **1** and **2** in aqueous environments. Dynamic light scattering (DLS) measurement of **1** in THF at 25 °C hardly showed scattering signals, while aggregates with an average size of 834 nm were visualized in water at 25 °C ([**1**] = 7.5 μM, Figure S1a in the Supporting Information). ^{1}H nuclear magnetic resonance (NMR) spectrum of **1** in THF-d_8 at 25 °C displayed signals at 8.29, 7.52, 7.21, and 6.70 ppm corresponding to the protons at the BPBP unit ([**1**] = 3.0 mM, Figure 2a). Upon addition of deuterated water, the aromatic signals showed upfield shift likely due to magnetic shielding effect by the self-assembled BPBP units (THF-d_8/D_2O = 90/10 and 50/50 v/v).[36,37] The absorption band of **1** showed a blue-shift upon addition of water, suggesting H-aggregate formation ([**1**] = 7.5 μM, 25 °C; 325 nm in THF, 321 nm in water; Figure 3a). The fluorescence spectra showed a significant red-shift of the emission band, from λ_{Em} = 410 nm in THF to 449 nm in water, which was accompanied by an emergence of a shoulder around 520 nm (λ_{Ex} = 330 nm, Figure 3c). Here, fluorescence anisotropy r of **1** decreased

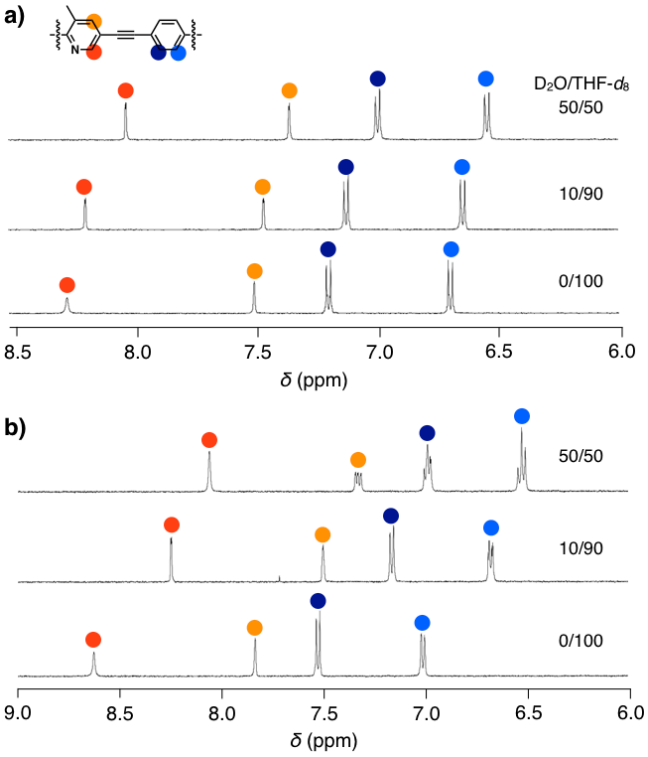

Figure 2. ^{1}H nuclear magnetic resonance spectra of (a) **1** and (b) **2** in the mixtures of D_2O and THF-d_8 at various ratios at 25 °C. [**1**] = 3.0 mM and [**2**] = 1.0 mM ([BPBP units] = 3.0 mM for both cases).

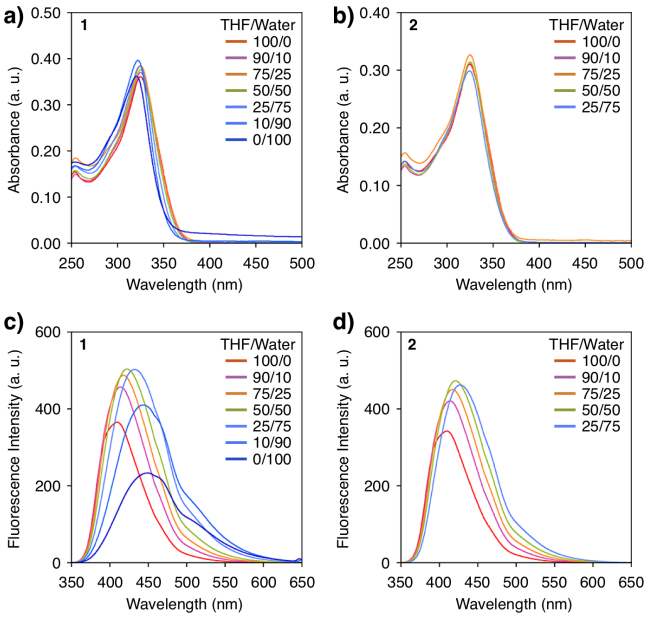

Figure 3. (a,b) Absorption and (c,d) fluorescence spectra of (a,c) **1** and (b,d) **2** in the mixtures of THF and water at 25 °C. The fluorescence spectra were measured upon excitation with 330 nm light for **1** and 328 nm light for **2**, respectively. Optical path length: 1.0 cm. [**1**] = 7.5 μM and [**2**] = 2.5 μM ([BPBP units] = 7.5 μM for both cases).

upon increment of the solvent polarity (r = 0.39 in THF, 0.18 in THF/water = 75/25, and 0.14 in water; [**1**] = 7.5 μM). In general, a slowly tumbling object, in other words a larger object, shows a larger fluorescence anisotropy value.[38] Since the solvent polarity increment elicited the aggregation formation, the observed decrease in fluorescence anisotropy indicates intermolecular energy transfer in the aggregates of **1**, namely, excimer formation of the BPBP unit of **1**. Excimer formation is also suggested from the significantly longer fluorescence lifetime (τ = 1.4 ns) at 550 nm in water than that at 450 nm (τ = 0.51 ns) in THF ([**1**] = 7.5 μM, Figure S2a,b). Analogous to **1**, the DLS and spectroscopic studies displayed that the assembly of the BPBP units of **2** is encouraged by increase in the solvent polarity (Figure 2b, 3b,d, also see Supporting Information Section 4 for details).

Introduction of MTM Mimics into Bilayer Membrane. Giant unilamellar vesicles (GUVs) of 1,2-dioleoyl-*sn*-glycero-3-phosphocholine (DOPC) containing **1** or **2** were prepared in 200 mM sucrose aq. by the gentle hydration method ([DOPC] = 200 μM, [**1**] = 20 μM, [**2**] = 6.7 μM, [BPBP units] = 20 μM for both cases).[39] Phase-contrast microscopy displayed successful formation of the GUVs in each case (Figure S3a,c). Fluorescent microscopy with an excitation light at 330–385 nm visualized spherical images for both DOPC•**1** and DOPC•**2** GUVs, indicating that **1** and **2** are embedded in the bilayer of DOPC (Figure S3b,d). Importantly, addition of 10 mM glucose aq. to the external aqueous phase of the vesicles resulted in membrane fluctuation of DOPC•**1** and DOPC•**2** GUVs (see Supporting Movies 1 and 2 for DOPC•**1** and DOPC•**2** GUVs, respectively). This observation suggests that glucose hardly passes through the DOPC bilayer containing **1** and **2**, which allows for regulation of an osmotic pressure by controlling the concentration difference of glucose across the bilayer.[40]

The location and orientation of **1** and **2** in the bilayer were studied by a fluorescence depth quenching method using phospholipids bearing a spin probe, where the efficiency of fluorescence quenching depends on the distance between the spin probe and a fluorescent chromophore (namely BPBP unit).[41] Three spin-labeled phospholipids, 1-palmitoyl-2-stearoyl-(X-doxyl)-*sn*-glycero-3-phosphocholine (X = 5: 5-Doxyl PC, X = 12: 12-Doxyl PC, and X = 16: 16-Doxyl PC), bearing a spin probe at different positions in the alkyl tail were used. Computational molecular modeling indicates that the spin probes of 5-, 12-, and 16-Doxyl PCs locate at 1.2, 0.6 and 0.2 nm away from the tip of the hydrophobic tail of DOPC, respectively (Figure S4). DOPC large unilamellar vesicles including **1** or **2** (DOPC•**1** LUV, DOPC•**2** LUV) with/without a Doxyl PC were prepared by freezing-and-thawing followed by extrusion through a 100-nm pore size membrane. Incorporation of 10-mol% 5-Doxyl PC into DOPC•**1** LUVs resulted in 51% decrease of the fluorescence intensity of **1** at 443 nm (λ_{Ex} = 325 nm, Figure S4a). Meanwhile, 10-mol% incorporation of 12- and 16-Doxyl PCs comparably quenched the fluorescence of **1** with higher efficiency than 5-Doxyl PC (65% and 67% decreases, respectively). Likewise, for DOPC•**2**-LUVs, 12-Doxyl and 16-Doxyl PCs comparably showed higher quenching efficiency for the fluorescence at 412 nm (λ_{Ex} = 325 nm; 62% and 65% decreases, respectively; Figure S4b) than 5-Doxyl PC (43%). The nearly comparable quenching efficiencies of 12- and 16-Doxyl PCs indicate that the BPBP units of **1** and **2** locate at the similar position with the spin probes of 12- and 16-Doxyl PCs inside the lipid bilayer, thereby suggesting that the BPBP units of **1** and **2** span the membrane. The lower quenching efficiency of 5-Doxyl PC than the others is likely due to the shorter length of the BPBP unit than the thickness of the hydrophobic layer of the DOPC bilayer.

Mechano-Responses of MTM Mimics in Membranes. Mechano-responses of membrane-embedded **1** and **2** to membrane tensions were assayed by applying an osmotic pressure $\Delta\Pi$ to the vesicles as performed in the previous studies.[42–44] The osmotic pressure $\Delta\Pi$ is controllable by the concentration difference ΔC of the solute (glucose) between the internal and external media of the vesicles as described below:

$$\Delta\Pi = \Delta CRT$$

$$\Delta C = C_{int} - C_{ext}$$

where R and T represent the gas constant and temperature, respectively.[40] On the basis of the Young-Laplace equation, an osmotic pressure causes a membrane tension $\Delta\sigma$ as described by the following equation:

$$\Delta\sigma = \frac{\Delta\Pi r}{2}$$

where r represents the radius of the vesicle. Since $\Delta\sigma$ correlates with r, different size vesicles were prepared under a controlled condition in the following study. Indeed, extrusion of DOPC liposomal suspensions containing **1** and **2** provided LUVs, and the size of the LUVs was successfully controlled by the pore size of the extrusion membrane (Small (*S*): 50 nm, Medium (*M*): 100 nm, and Large (*L*): 200 nm). By the extrusion through a 100-nm pore size membrane, DOPC•**1** LUV^M and DOPC•**2** LUV^M with average sizes of 135 nm and 147 nm were prepared in 200 mM glucose aq., respectively ([**1**]/[DOPC] = 0.050, [**2**]/[DOPC] = 0.017, [DOPC] = 0.20 mM, [BPBP units] = 10 μM for both LUVs; Figure 4f). The obtained DOPC•**1** LUV^M showed fluorescence at λ_{FL} = 443 nm (λ_{Ex} = 325 nm, Figures 4a and S5a, blue solid line). The red-shifted fluorescence of **1** compared to that in THF (λ_{FL} = 410 nm, Figures 4a and S5a, black dotted line) suggests that the BPBP unit of **1** forms intermolecular self-assembly in the bilayer. On the other hand, DOPC•**2** LUV^M showed fluorescence at 412 nm, suggesting that the stacking of the BPBP units of **2** in the bilayer is much weaker than those of **1** (Figures 4b and S5b, blue solid line). Upon increase in tension to $\Delta\sigma$ = 20 mN m^{-1} to expand the membrane, DOPC•**1** LUV^M displayed blue-shift of the fluorescence band with decrease in the excimer emission intensity (λ_{FL} = 443 nm at $\Delta\sigma$ = 0 mN m^{-1}, 434 nm at 20 mN m^{-1}; Figures 4a and S5a, black solid line), while the contracting tension prompted red-shift of the fluorescence band with intensified excimer emission (λ_{FL} = 445 nm at $\Delta\sigma$ = –34 mN m^{-1}, Figures 4a and S5a, red dashed line). Importantly, upon increase in tension to expand the membrane, DOPC•**1** LUV^M showed increment in the fluorescence anisotropy r, while its size was almost constant (r = 0.18 at $\Delta\sigma$ = –34 mN m^{-1}, 0.19 at 0 mN m^{-1}, 0.22 at 20 mN m^{-1}). These observations indicate that the degree of intermolecular energy transfer decreases due to dissociation of self-assembled **1** molecules. Namely, **1** responds to the expanding and contracting tensions by dissociation and association of the BPBP units, respectively.[45] Here, 100-fold dilution of **1** in DOPC•**1** LUV^M ([**1**]/[DOPC] = 0.00050) resulted in slightly blue-shifted fluorescence peaks at 441 nm at 0 mN m^{-1} and 432 nm at 20 mN m^{-1} (Figure S6a), respectively. This concentration-dependent

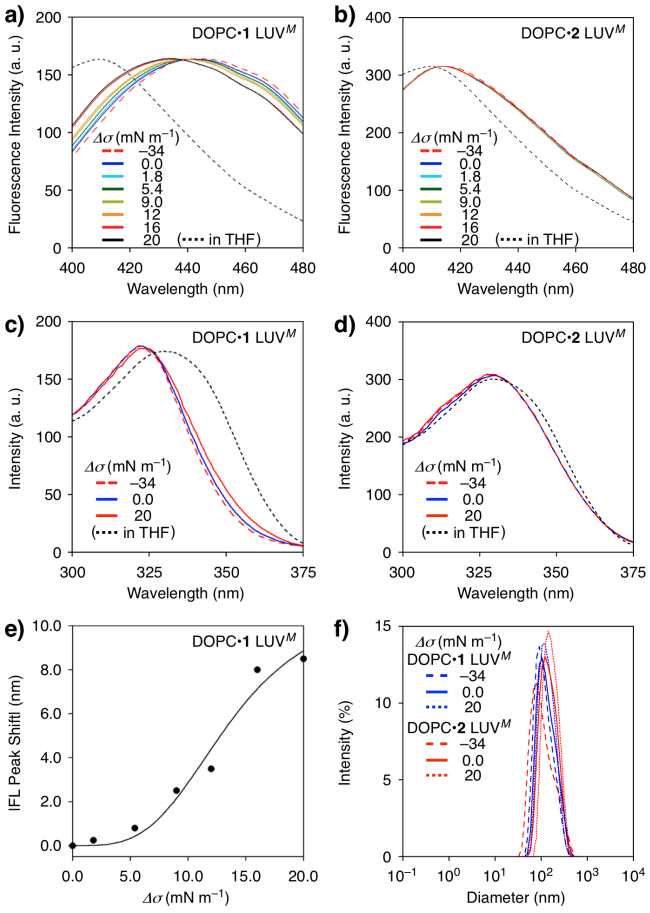

Figure 4. (a,b) Fluorescence and (c,d) excitation spectra of (a,c) DOPC•**1** and (b,d) DOPC•**2** LUV^{M}s in water (solid and dashed lines) under varying membrane tensions and in THF (black dotted lines) at 25 °C. The fluorescence spectra were measured upon excitation with 325 nm light. The excitation spectra were measured monitoring the fluorescence at 440 nm. [**1**]/[DOPC] = 0.050, [**2**]/[DOPC] = 0.017 ([BPBP units] = 10 μM for both cases), [DOPC] = 0.20 mM. The whole spectra (375–600 nm) of (a) and (b) are displayed in the Supporting Figure S5a,b. (e) Absolute values of the fluorescence peak shift of DOPC•**1** LUV^M from λ_{FL} = 443 nm at $\Delta\sigma$ = 0 mN m^{-1} in water as a function of the membrane tension. The plot was analyzed by curve-fitting with Hill equation (R = 0.9868). (f) Volume-averaged DLS profiles of DOPC•**1** LUV^M (blue) and DOPC•**2** LUV^M (red) in water under tensionless (solid lines) and tensioned (–34 mN m^{-1}: dashed lines, 20 mN m^{-1}: dotted lines) conditions. [**1**]/[DOPC] = 0.050, [**2**]/[DOPC] = 0.017 ([BPBP units] = 10 μM for both cases), [DOPC] = 0.20 mM. Mean hydrodynamic diameters: (DOPC•**1** LUV^M) 129 nm at –34 mN m^{-1}, 135 nm at 0 mN m^{-1}, 143 nm at 20 mN m^{-1}, (DOPC•**2** LUV^M) 126 nm at –34 mN m^{-1}, 147 nm at 0 mN m^{-1}, 171 nm at 20 mN m^{-1}.

fluorescence change is likely due to intermolecular stacking of the BPBP unit. Fluorescence spectra of **2** in the bilayer showed much smaller shift from the fluorescence in THF compared to **1**, and hardly showed responses to the membrane tensions (Figures 4b and S5b). Importantly, 100-fold dilution of **2** in DOPC•**2** LUV^M ([**2**]/[DOPC] = 0.00017) also hardly influenced the fluorescence wavelength regardless of the strength of the applied tensions (λ_{FL} = 412 nm, Figure S6b). These results suggest that the weak intramolecular stacking of the BPBP units mainly dictates the slight shift of the fluorescence band of **2**, where emission wavelength is mostly insensitive to the membrane tensions. In addition to the fluorescence spectral change mentioned above, the excitation spectrum of DOPC•**1** LUV^M displayed red-shift (disassembly) and blue-shift (assembly) in response to the expanding and contracting tensions, respectively (Figure 4c). In contrast, DOPC•**2** LUV^M hardly showed changes in the excitation spectrum in response to the tensions (Figure 4d). Hence, the membrane tension elicits the changes in the intermolecular stacking of the BPBP units of **1** at the ground state, while initial intramolecular stacking of the BPBP units in **2** is likely too weak for the detection of the tension-triggered conformational changes by the spectroscopic analyses.

The fluorescence-spectral responses of **1** and **2** in DOPC bilayer to the tension hardly depend on the curvature of the LUV. DOPC•**1** LUVs with smaller and larger sizes showed fluorescence at 443 nm with similar spectral profile to DOPC•**1** LUV^M (DOPC•**1** LUV^S: 82 nm, DOPC•**1** LUV^L: 175 nm; [**1**]/[DOPC] = 0.050, [DOPC] = 0.20 mM, Figure S5c,d). Upon exposure to the osmotic pressures to induce membrane tensions to $\Delta\sigma$ = 20 and –34 mN m^{-1}, DOPC•**1** LUV^S and DOPC•**1** LUV^L showed blue- and red-shifts of the fluorescence in a similar manner to DOPC•**1** LUV^M, respectively. Meanwhile, almost unchanged fluorescence spectra were observed in any sizes of DOPC•**2** LUVs (Figure S5e,f).

Mechano-Sensitive Ion Transportation in Liposomal and Black-Lipid Membranes. Previous studies in our group[30,32] revealed that the assembly of the membrane spanning amphiphiles allows for ion transportation[46–53] by forming supramolecular channels. Since above-mentioned fluorescence study indicated the tension-responsive dissociation/association of the BPBP units of **1**, we expected that the membrane tension could modulate the ion transportation function. At first, ion transportation of **1** and **2** was investigated on the vesicles by monitoring a fluorescence intensity change using a pH sensitive probe. DOPC•**1** LUV^M encapsulating 8-hydroxypyrene-1,3,6-trisulfonate (HPTS) in the internal aqueous phase was prepared in 20 mM HEPES buffer containing 50 mM KCl at pH 7.1 (DOPC•**1** LUV^M⊃HPTS, [**1**]/[DOPC] = 0.050). HPTS emits 510-nm fluorescence upon excitation with 450-nm light at pH higher than 5, and the fluorescence intensity increases upon enhancement of pH.[54] Under the tensionless condition or exposure to the contracting tension, DOPC•**1** LUV^M⊃HPTS hardly showed increment of the fluorescence intensity upon addition of KOH ($\Delta\sigma$ = 0.0 or –34 mN, Figure 5a, blue thick and dotted lines, respectively). In sharp contrast, under exposure to the expanding tension, DOPC•**1** LUV^M⊃HPTS displayed elevation of the fluorescence intensity readily upon addition of KOH ($\Delta\sigma$ = 20 mN, Figure 5a, blue thin line), indicating the transportation of potassium ions into the vesicles to raise the intravesicular pH. The Hill analysis on the concentration dependency of the cation transportation rate afforded the Hill coefficient n = 2.98 ± 0.26 (R = 0.993), suggesting supramolecular ion channel formation of **1**, possibly by the trimeric assembly (Figure 5b, blue thin line).[55] On the other hand, DOPC•**2** LUV^M⊃HPTS showed a rapid increase in the fluorescence intensity upon addition of KOH even under the absence of osmotic pressure (Figure 5a, red thick line; [**2**]/[DOPC] = 0.017). However, interestingly, while similar fluorescence enhancement was observed under the contracting tension ($\Delta\sigma$ = –34 mN m^{-1}, Figure 5a, red dotted line), the expanding tension caused a significant decline of

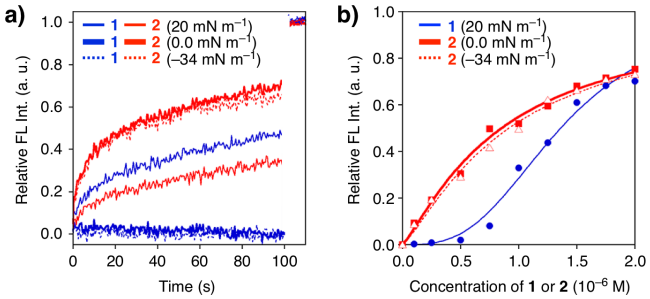

Figure 5. (a) Changes in fluorescence intensity of HPTS encapsulated in DOPC•**1** and DOPC•**2** LUV^{M}s in HEPES buffer at 20 °C as a function of time after the addition of KOH at 0 sec followed by addition of 1.0 wt% triton X-100 at 100 sec ([DOPC] = 0.20 mM, [**1**] = 1.0 μM, [**2**] = 0.33 μM, [HPTS] = 30 μM, 20 mM HEPES, 50 mM KCl, pH 7.1, excitation at 460 nm, emission at 510 nm). ΔpH = 0.8 (7.1 to 7.9). Tensions added to DOPC•**1** LUV^{M}⊃HPTS (blue lines) and DOPC•**2** LUV^{M}⊃HPTS (red lines): 0 (thick lines), 20 (thin lines) and –34 mN m^{-1} (dotted lines). (b) Plots of relative 510-nm fluorescence intensities of HPTS encapsulated in DOPC•**1** and DOPC•**2** LUV^{M}s at 30 s after the addition of KOH in 20 mM HEPES buffer containing 50 mM KCl at 20 °C as a function of concentration of **1** and **2**. Curve-fitting analyses were carried out by the Hill equation (R = 0.993 (DOPC•**1** LUV^{M} at 20 mN m^{-1}), 0.996 (DOPC•**2** LUV^{M} at 0.0 mN m^{-1}), 0.995 (DOPC•**2** LUV^{M} at –34 mN m^{-1})). Colors and line types correspond to those in (a).

the ion transportation rate ($\Delta\sigma$ = 20 mN m^{-1}, Figure 5a, red thin line). The Hill coefficients of **2** under the tensionless and contracting-tension conditions were evaluated to be 1.22 ± 0.07 (R = 0.996) and 1.27 ± 0.03 (R = 0.995), respectively, suggesting formation of the unimolecular channel as the major active species (Figure 5b, red thick and dotted lines, respectively). It should be mentioned that DOPC LUV^{M}⊃HPTS without **1** or **2** showed no ion transportation at any tensions (Figure S7a). Thus, it was demonstrated that **1** responds to the expanding tension to prompt the ion transportation by forming a supramolecular ion channel, while **2** shows ion transportation through a unimolecular ion channel under the tensionless condition and responds to the expanding tension to reduce the transportation rate likely by closing or collapsing the ion channel.[56]

For further detailed investigation on the mechanosensitive ion transporting behaviors by direct detection of the ion transportation, **1** and **2** were embedded into a DOPC black lipid membrane (BLM) containing *n*-decane. The BLM is formed horizontally at the bottom of the upper chamber containing electrolyte buffer solution. Membrane tension $\Delta\sigma$ to expand the BLM was applied by hydrostatic pressure produced by the difference in the height Δh of the solution surfaces between the upper and lower chambers. Microscopic fluorescence spectroscopy of **1** in BLM displayed a blue-shift of the fluorescence peak λ_{FL} from 443 nm to 436 nm upon increase in Δh from 1.0 mm to 9.0 mm (λ_{Ex} = 295–347 nm, Figure S9). Here, on the basis of the relationship between membrane tension $\Delta\sigma$ and fluorescence band λ_{FL} of **1** in DOPC bilayer (Figure 4e), the membrane tension $\Delta\sigma$ in the BLM system caused by Δh could be estimated by the microscopic fluorescence spectroscopic analysis.

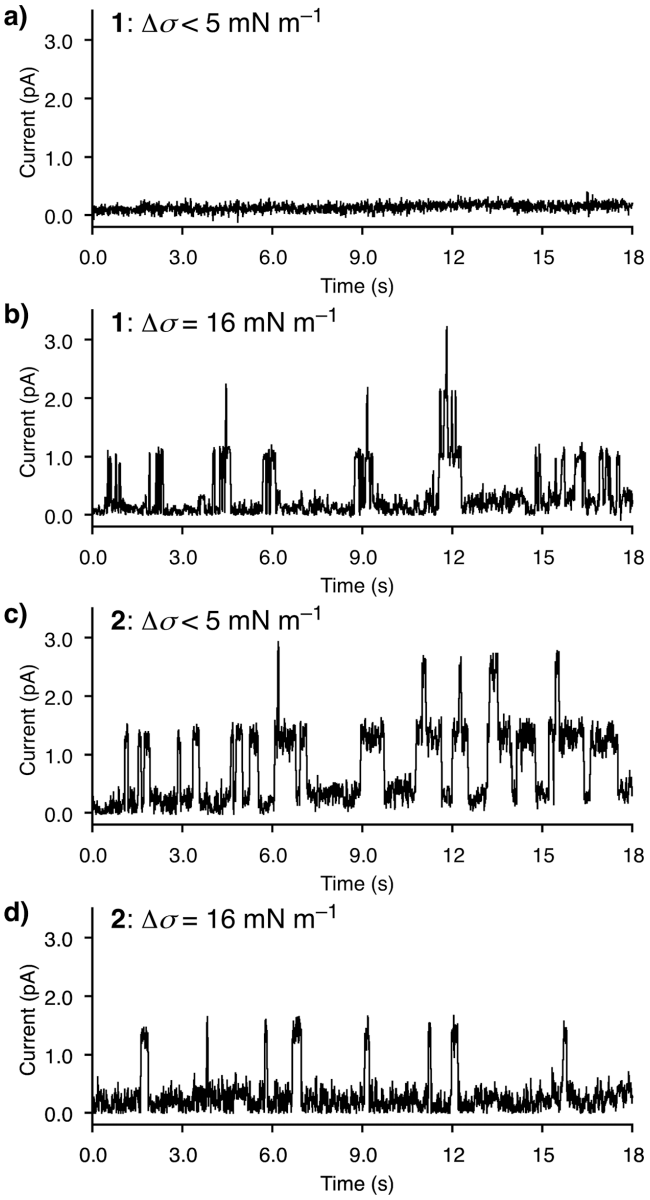

Figure 6. Current traces at the applied voltage of 120 mV of a DOPC BLM containing (a,b) **1** or (c,d) **2** ([**1**]/[DOPC] = 0.010, [**2**]/[DOPC] = 0.0033) in HEPES buffer (20 mM HEPES, 50 mM KCl, 2.0 mM $MgCl_2$, pH 7.5) under (a,c) low tension ($\Delta\sigma$ < 5 mN m^{-1}) or (b,d) increased expanding tension ($\Delta\sigma$ = 16 mN m^{-1}) at 20 °C.

Ion transportation through the BLM was directly detected in real time as a current between the electrodes in the upper and lower chambers. At a low-tension condition ($\Delta\sigma$ < 5 mN m^{-1}), **1** hardly showed current flow, while **2** exhibited significant current flows (Figure 6a,c). A rise of the expanding tension to 16 mN m^{-1} triggered ion transportation of **1** (Figure 6b), which is in line with the trend observed in the DOPC•**1** LUV^{M}⊃HPTS system (Figure. 5a, blue thin line). At the expanding tension of 16 mN m^{-1}, **2** showed a significantly reduced frequency of the current flow (Figure 6d; 4.3-times reduction in average compared to the low-tension condition), which is also consistent with the result observed in the DOPC•**2** LUV^{M}⊃HPTS system (Figure 5a, red thin line). It should be mentioned here that DOPC bilayer in the BLM sys-

tem without **1** or **2** hardly showed ion transportation at any tensions under these experimental conditions, indicating that **1** and **2** function to transport ions (Figure S10).

Under the ion-transporting conditions, **2** showed a higher conductance than **1** (**1**: g = 8.2 pS, **2**: 12 pS). The voltage-clamp traces of **1** and **2** in DOPC BLM show "square-top" shape of the current flow, where the current abruptly switches between two modes, off- and on-states maintaining constant current intensities. Such a profile is typically observed in the case of ion transportation by ion channels,[55,57] thereby suggesting the formation of ion channels by **1** and **2**. It is known that the channel diameter d correlates with conductance g on the basis of the Hille equation,[58]

$$\frac{1}{g} = \frac{l\rho}{\pi(d/2)^2} + \frac{\rho}{d}$$

where l and ρ are the length of channel (3.5 nm) and the resistivity of recording solution (2.35 Ω m), respectively. Analyses on the Hille equation including the Sansom correction factor[59] revealed d of **1** and **2** to be *ca*. 0.74 and 0.92 nm, respectively.[60]

Here, it would be significant to discuss about the difference in the responses of **1** and **2** to the expanding and contracting tensions. It is known that the increase in the expanding tension enhances the membrane fluidity.[34] Under the tensionless and contracting-tension conditions, where the mobility of the lipid molecules is relatively restricted, the fluorescence study of **1** visualized the formation of the developed intermolecular π-π stacking of the BPBP units in the lipid bilayer, which likely stabilizes closely-stacked assemblies rather than the formation of the pore-forming channels (Figure 4a, blue solid and red dashed lines; Figure 7a (i) and (ii)). By rise of the membrane expanding tension to increase the mobility of the lipid molecules, the intermolecular stacking is attenuated, as was visualized by the fluorescence study (Figure 4a, black solid line). It is likely that the increase in the mobility of the BPBP units allows for the formation of a supramolecular channel with a short life-span (milli-second order) (Figure 5a, blue thin line; Figures 6b, 7a (iii)). In contrast, as described above, the stacking of the BPBP units of **2** in the bilayer would be much less efficient compared to those of **1** under the tensionless condition (Figure 4b, blue line), suggesting the restricted geometry of the BPBP units. The less efficient stacking of the BPBP units would permit a certain degree of mobility of each BPBP unit to allow for the tentative formation of a channel (Figure 5a, red thick line; Figures 6c, 7b (ii)), while the restriction of the geometry likely inhibits closer packing in response to the contracting tension (Figure 5a, red dotted line; Figure 7b (i)). On the other hand, the enhanced mobility of the membrane due to the expanding tension likely causes further increase in the flexibility of the BPBP units to rather destabilize the channel structure (Figure 5a, red thin line; Figures 6d, 7b (iii)).

Finally, it would be interesting to make a comparison between the present systems with the biological mechano-sensitive ion channels. The rupture force to dissociate intermolecular stacking of the BPBP unit of **1** could be estimated on the basis of the tension-induced fluorescence shift. The dependence of the fluorescence peak shift of DOPC•**1** LUV^{M} on the expanding tension displayed a sigmoidal profile ([**1**]/[DOPC] = 0.050, [DOPC] = 0.20 mM, Figure 4e). The curve-fitting analysis with Hill equation revealed that the tension causing 50% fluorescence peak shift, regarded as the average rupture force, is 13.6 mN m^{-1}. The bacterial MSC proteins, MscS and MscL, are known to operate at tensions of 5.5 mN m^{-1} and 12 mN m^{-1} to open the channel, respectively, where they play roles as safety valves to prevent the cells from lysis.[61,62] It is of interest that **1** senses a similar amplitude of tension to MscL, although their molecular structures and sizes are largely different from each other. The conductance measurement of **2** also suggested that **2** operates at similar tensions to MSC proteins. Another interesting point is that while both MSC proteins and **1** form supramolecular ion channels and sense the expanding tension to trigger ion transportation in common, **2** forming a unimolecular channel shows the contrasting response to the expanding tension to deactivate the ion transportation.

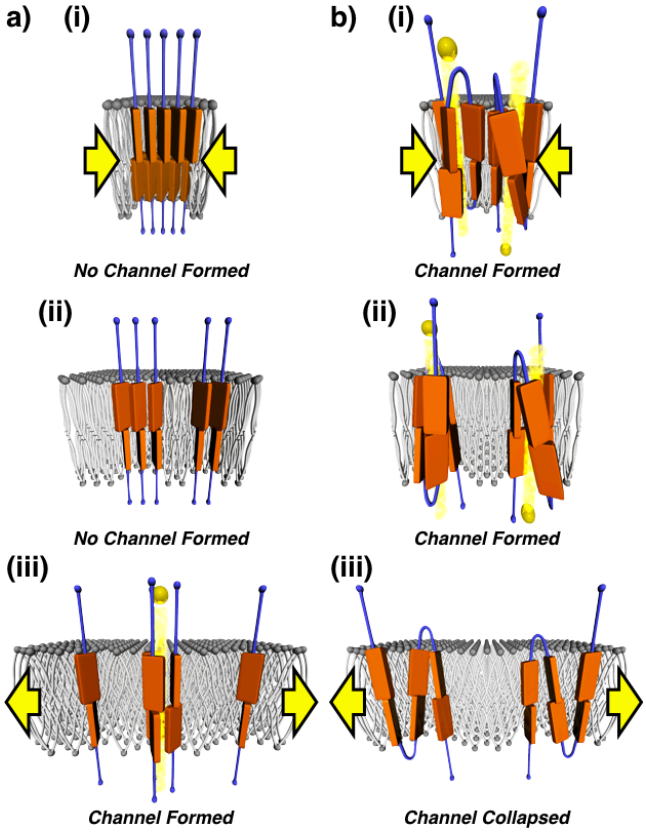

Figure 7. Schematic illustrations displaying the responses of (a) **1** and (b) **2** to (i) membrane contraction and (iii) expansion from (ii) a tensionless condition in a DOPC bilayer. Orange, blue and gray parts denote the hydrophobic and hydrophilic parts in **1** and **2** and DOPC, respectively. Yellow spheres represent a cation. Yellow arrows depict the direction of membrane tension.

SUMMARY

We demonstrated the mechano-sensitive synthetic ion channels consisting of membrane-spanning amphiphiles **1** and **2**, where the tension triggers changes in the conformation and self-assembly of the amphiphiles, and modulates ion transportation. The BPBP unit of **1** forms intermolecular self-assembly in the bilayer, which dissociate and associate in response to the expanding and contracting tensions, respectively. While **1** hardly shows ion transportation under the tensionless or the contracting-tension conditions, **1** responds to the expanding tension to prompt the ion transportation by forming a supramolecular ion channel. The BPBB units of **2**, on the

other hand, form weak intramolecular stacking. **2** shows ion transportation through a unimolecular ion channel under the tensionless condition and responds to the expanding tension to reduce the transportation activity likely by closing or collapsing the ion channel. The operating force of these membrane-spanning amphiphiles indicates that the amplitude of the tension sensed by the amphiphiles is similar to those sensed by the MSC proteins. It is known that the MSC protein opens its pore by membrane expanding force, which works as a molecular device for tactile and auditory senses. We believe that this study opens the door to the development of membrane-embedded synthetic molecular devices responsive to external physical stimuli for bio-related applications.

METHODS

Giant Unilamellar Vesicles Preparation. To a mixture of $CHCl_3$/MeOH (2/1 v/v, 10 μL) was put in a glass test tube, was added a $CHCl_3$ solution of DOPC (2.0 mM, 20 μL), a MeOH solution of glucose (10 mM, 12 μL) and a CH_2Cl_2 solution of an MTM mimic (**1**: 0.10 mM, 40.0 μL, or **2**: 0.10 mM, 13.3 μL). The resulting mixture was gently dried under Ar flow to produce thin lipid film. The film was subsequently dried under vacuum over 3 h at 25 °C and hydrated overnight with 200 mM sucrose aq. (200 μL) under Ar at 37 °C.

Large Unilamellar Vesicles Preparation. To a mixture of $CHCl_3$/MeOH (2/1 v/v, 50 μL) put in a glass test tube, were added a $CHCl_3$ solution of DOPC (2.0 mM, 100 μL) and a CH_2Cl_2 solution of an MTM mimic. The resulting mixture was gently dried under Ar flow to produce thin lipid film, which was subsequently dried under vacuum over 3 h at 25 °C and hydrated overnight with 200 mM glucose aq. (1.0 mL) under Ar at 37 °C. The resulting mixture was stirred on a shaker (203 min^{-1}) for 1 h at 37 °C, followed by vortex mixing for 10 s, freezing-and-thawing for three times, and subsequent vortex mixing for 10 s. After being left standing overnight at 37 °C, the resulting mixture was passed through a polycarbonate membrane of defined pore size (50 nm: LFM-50, 100 nm: LFM-100 or 200 nm: LFM-200) attached in a LiposoFast-Basic device by pushing the sample back and forth between the two gas-tight syringes over 11 times.

LUV^Ms for fluorescence depth quenching were prepared by following the above procedure using a mixture of DOPC and 5-Doxyl PC, 12-Doxyl PC, or 16-Doxyl PC ([DOPC]/[Doxyl PC] = 90/10).

LUV^Ms encapsulating HPTS in the inner aqueous phase were prepared by following the above procedure, where 20 mM HEPES buffer containing 50 mM KCl (pH 7.1) and 30 μM HPTS was used as the hydration medium. After the extrusion process, the obtained suspension was dialyzed at 4 °C in 20 mM HEPES buffer containing 50 mM KCl (pH 7.1, 1.0 L, three times) using Spectra/Por Dialysis Membrane (MWCO 3500).

The osmotic pressure $\Delta\Pi$ to LUVs was controlled by the concentration difference (ΔC) of glucose between the internal and external media of the LUVs. Appling tension higher than 20 mN m^{-1} or lower than –34 mN m^{-1} resulted in little scattering or polydispersed particle size distribution profiles in DLS, suggesting disruption or deformation of LUVs.

Fluorescence Measurement for Ion Transportation Study. To a DOPC•**1** LUV^Ms⊃HPTS or DOPC•**2** LUV^Ms⊃HPTS suspension ([DOPC] = 0.20 mM, [HPTS] = 30 μM) in 20 mM HEPES buffer containing 50 mM KCl (1.99 mL, pH 7.1) was added an aqueous solution of KOH (0.60 M, 10 μL, ΔpH = 0.8) by a syringe in the dark at 20 °C. Fluorescence intensity of HPTS at 510 nm upon excitation with 460 nm-light was monitored as a function of time until the addition of 1.0 wt% Triton X-100 (40 μL) at 100 s. Relative fluorescence intensity of HPTS in response to the pH enhancement was evaluated by the equation of

$$I = \frac{I_t - I_0}{I_{lyzed} - I_0}$$

where I_0, I_t and I_{lyzed} represent the fluorescence intensities before addition of KOH, at t seconds after addition of KOH, and after lysis by the addition of 1.0 wt% Triton X-100, respectively.

Conductance Measurements and Tension Calculation in BLM System. Planar lipid bilayer was prepared by the reported procedure.[63] A mixture of DOPC (12.7 mM, 100 μL) in $CHCl_3$ and an MTM mimic (**1**: 1.0 mM, 12.5 μL, or **2**: 0.10 mM, 42 μL) in CH_2Cl_2 was gently dried under N_2 flow, which was then dispersed in *n*-decane (100 μL) and was painted on an orifice (diameter 150 μm) sandwiched by two chambers containing HEPES buffer (upper chamber: *trans*, lower chamber: *cis*, 20 mM HEPES, 50 mM KCl, 2.0 mM $MgCl_2$, pH 7.5, 0.30 mL each). Current was measured with a Nihon Kohden CEZ2400 amplifier and stored on a computer using an AD Instruments PowerLab at 40 kHz sampling rate. Recordings were filtered at 1 kHz. All the current recordings were performed at 20 °C. Membrane tension $\Delta\sigma$ was applied by hydrostatic pressure to expand the planar membrane, where the hydrostatic pressure was produced by the difference in height Δh of the water surface between the two chambers.

ASSOCIATED CONTENT

Supporting Information. Materials; Instrumentation; Synthesis; Self-Assembly of **2**; DLS and Fluorescence Lifetime Measurements of **1** and **2**; Optical Microscopic Observations of DOPC•**1** and DOPC•**2** GUVs; Fluorescence Depth Quenching Studies, Size- and Concentration-Dependencies of Fluorescence Spectral Profiles, HPTS Assays with Different Cations, DLS Measurements of DOPC•**1** and DOPC•**2** LUVs; Microscopic Fluorescence Spectroscopic Measurements of DOPC•**1** BLM; Conductance Measurements of DOPC BLM. Movies of the fluctuating DOPC•**1** and DOPC•**2** GUVs upon addition of glucose aq. This material is available free of charge via the Internet at http://pubs.acs.org.

AUTHOR INFORMATION

Corresponding Author

kkinbara@bio.titech.ac.jp

ACKNOWLEDGMENT

This work was partially supported by Grant-in-Aid for Scientific Research B (16H04129 to KK), Yamada Science Foundation (KK), Grant-in-Aid for Scientific Research on Innovative Areas "π-System Figuration (No.2601)" (26102001 to TM), JST PRESTO program "Molecular Technology and Creation of New Functions" (TM), and the Management Expenses Grants for National Universities Corporations from MEXT.

REFERENCES

(1) Chen, W.; Horike, S.; Umeyama, D.; Ogiwara, N.; Itakura, T.; Tassel, C.; Goto, Y.; Kageyama, H.; Kitagawa, S. *Angew. Chem. Int. Ed.* **2016**, *55*, 5195–5200.

(2) Li, J.; Nagamani, C.; Moore, J. S. *Acc. Chem. Res.* **2015**, *48*, 2181–2190.
(3) Imato, K.; Irie, A.; Kosuge, T.; Ohishi, T.; Nishihara, M.; Takahara, A.; Otsuka, H. *Angew. Chem. Int. Ed.* **2015**, *54*, 6168–6172.
(4) Yagai, S.; Okamura, S.; Nakano, Y.; Yamauchi, M.; Kishikawa, K.; Karatsu, T.; Kitamura, A.; Ueno, A.; Kuzuhara, D.; Yamada, H.; Seki, T.; Ito, H. *Nat. Commun.* **2014**, *5*, 4013.
(5) Balkenende, D. W. R.; Coulibaly, S.; Balog, S.; Simon, Y. C.; Fiore, G. L.; Weder, C. *J. Am. Chem. Soc.* **2014**, *136*, 10493–10498.
(6) Liu, G.; Liu, J.; Liu, Y.; Tao, X. *J. Am. Chem. Soc.* **2014**, *136*, 590–593.
(7) Baláž, P.; Achimovičová, M.; Baláž, M.; Billik, P.; Cherkezova-Zheleva, Z.; Criado, J. M.; Delogu, F.; Dutková, E.; Gaffet, E.; Gotor, F. J.; Kumar, R.; Mitov, I.; Rojac, T.; Senna, M.; Streletskii, A.; Wieczorek-Ciurowa, K. *Chem. Soc. Rev.* **2013**, *42*, 7571–7637.
(8) Takacs, L. *Chem. Soc. Rev.* **2013**, *42*, 7649–7659.
(9) Nagura, K.; Saito, S.; Yusa, H.; Yamawaki, H.; Fujihisa, H.; Sato, H.; Shimoikeda, Y.; Yamaguchi, S. *J. Am. Chem. Soc.* **2013**, *135*, 10322–10325.
(10) Larsen, M. B.; Boydston, A. J. *J. Am. Chem. Soc.* **2013**, *135*, 8189–8192.
(11) Chen, Y.; Spiering, A. J. H.; Karthikeyan, S.; Peters, G. W. M.; Meijer, E. W.; Sijbesma, R. P. *Nat. Chem.* **2012**, *4*, 559–562.
(12) Chi, Z.; Zhang, X.; Xu, B.; Zhou, X.; Ma, C.; Zhang, Y.; Liu, S.; Xu, J. *Chem. Soc. Rev.* **2012**, *41*, 3878–3896.
(13) Huang, Z.; Boulatov, R. *Chem. Soc. Rev.* **2011**, *40*, 2359–2384.
(14) Black, A. L.; Lenhardt, J. M.; Craig, S. L. *J. Mater. Chem.* **2011**, *21*, 1655–1663.
(15) Sagara, Y.; Kato, T. *Angew. Chem. Int. Ed.* **2011**, *50*, 9128–9132.
(16) Caruso, M. M.; Davis, D. A.; Shen, Q.; Odom, S. A.; Sottos, N. R.; White, S. R.; Moore, J. S. *Chem. Rev.* **2009**, *109*, 5755–5798.
(17) Davis, D. A.; Hamilton, A.; Yang, J.; Cremar, L. D.; Gough, D. V.; Potisek, S. L.; Ong, M. T.; Braun, P. V.; Martínez, T. J.; White, S. R.; Moore, J. S.; Sottos, N. R. *Nature* **2009**, *459*, 68–72.
(18) Haswell, E. S.; Phillips, R.; Rees, D. C. *Structure* **2011**, *19*, 1356–1369.
(19) Dal Molin, M.; Verolet, Q.; Colom Diego, A.; Letrun, R.; Derivery, E.; Gonzalez-Gaitan, M.; Vauthey, E.; Roux, A.; Sakai, N.; Matile, S. *J. Am. Chem. Soc.* **2015**, *137*, 568–571.
(20) Verolet, Q.; Soleimanpour, S.; Fujisawa, K.; Molin, M. D.; Sakai, N.; Matile, S. *ChemistryOpen* **2015**, *4*, 264–267.
(21) Doval, D. A.; Molin, M. D.; Ward, S.; Fin, A.; Sakai, N.; Matile, S. *Chem. Sci.* **2014**, *5*, 2819–2825.
(22) Doval, D. A.; Matile, S. *Org. Biomol. Chem.* **2013**, *11*, 7467–7471.
(23) Fin, A.; Jentzsch, A. V.; Sakai, N.; Matile, S. *Angew. Chem. Int. Ed.* **2012**, *51*, 12736–12739.
(24) Ishikawa, D.; Mori, T.; Yonamine, Y.; Nakanishi, W.; Cheung, D. L.; Hill, J. P.; Ariga, K. *Angew. Chem. Int. Ed.* **2015**, *54*, 8988–8991.
(25) Sakakibara, K.; Joyce, L. A.; Mori, T.; Fujisawa, T.; Shabbir, S. H.; Hill, J. P.; Anslyn, E. V.; Ariga, K. *Angew. Chem. Int. Ed.* **2012**, *51*, 9643–9646.
(26) Mori, T.; Okamoto, K.; Endo, H.; Hill, J. P.; Shinoda, S.; Matsukura, M.; Tsukube, H.; Suzuki, Y.; Kanekiyo, Y.; Ariga, K. *J. Am. Chem. Soc.* **2010**, *132*, 12868–12870.
(27) Michinobu, T.; Shinoda, S.; Nakanishi, T.; Hill, J. P.; Fujii, K.; Player, T. N.; Tsukube, H.; Ariga, K. *J. Am. Chem. Soc.* **2006**, *128*, 14478–14479.
(28) Kim, J.; Swager, T. M. *Nature* **2001**, *411*, 1030–2034.
(29) Muraoka, T.; Kinbara, K. *Chem. Commun.* **2016**, *52*, 2667–2678.
(30) Muraoka, T.; Endo, T.; Tabata, K. V.; Noji, H.; Nagatoishi, S.; Tsumoto, K.; Li, R.; Kinbara, K. *J. Am. Chem. Soc.* **2014**, *136*, 15584–15595.
(31) Shima, T.; Muraoka, T.; Hoshino, N.; Akutagawa, T.; Kobayashi, Y.; Kinbara, K. *Angew. Chem. Int. Ed.* **2014**, *53*, 7173–7178.
(32) Muraoka, T.; Shima, T.; Hamada, T.; Morita, M.; Takagi, M.; Tabata, K. V.; Noji, H.; Kinbara, K. *J. Am. Chem. Soc.* **2012**, *134*, 19788–19794.
(33) Muraoka, T.; Shima, T.; Hamada, T.; Morita, M.; Takagi, M.; Kinbara, K. *Chem. Commun.* **2011**, *47*, 194–196.
(34) Lehtonen, J. Y. A.; Kinnunen, P. K. J. *Biophys. J.* **1994**, *66*, 1981–1990.
(35) Birckner, E.; Grummt, U.-W.; Göller, A. H.; Pautzsch, T.; Egbe, D. A. M.; Al-Higar, M.; Klemm, E. *J. Phys. Chem. A* **2001**, *105*, 10307–10315.
(36) Hunter, C. A.; Lawson, K. R.; Perkins, J.; Urch, C. J. *J. Chem. Soc., Perkin Trans. 2* **2001**, 651–669.
(37) Ishida, T.; Ibe, S.; Inoue, M. *J. Chem. Soc., Perkin Trans. 2* **1984**, 297–304.
(38) Lakowicz, J. R. *Principles of Fluorescence Spectroscopy*, 3rd ed.; Springer: New York,, 2006.
(39) Akashi, K.; Miyata, H.; Itoh, H.; Kinosita, K., Jr. *Biophys. J.* **1996**, *71*, 3242–3250.
(40) Hamada, T.; Kishimoto, Y.; Nagasaki, T.; Takagi, M. *Soft Matter* **2011**, *7*, 9061–9068.
(41) Weiss, L. A.; Sakai, N.; Ghebremariam, B.; Ni, C.; Matile, S. *J. Am. Chem. Soc.* **1997**, *119*, 12142–12149.
(42) Saleem, M.; Morlot, S.; Hohendahl, A.; Manzi, J.; Lenz, M.; Roux, A. *Nat. Commun.* **2015**, *6*, 6249.
(43) Köttgen, M.; Buchholz, B.; Garcia-Gonzalez, M. A.; Kotsis, F.; Fu, X.; Doerken, M.; Boehlke, C., Steffl, D.; Tauber, R.; Wegierski, T.; Nitschke, R.; Suzuki, M.; Kramer-Zucker, A.; Germino, G. G.; Watnick, T.; Prenen, J.; Nilius, B.; Kuehn, E. W.; Walz, G. *J. Cell Biol.* **2008**, *182*, 437–447.
(44) Yu, W. G.; Sokabe, M. *Jpn. J. Physiol.* **1997**, *47*, 553–565.
(45) It is unlikely that the fluorescence spectral change of **1** in response to applied membrane tension is due to the conformational change, because the tension-dependent change in the fluorescence anisotropy of DOPC•**1** LUV^{M} should be caused mainly by association and dissociation of **1** changing the degree of energy transfer.
(46) Sakai, N.; Matile, S. *Langmuir* **2013**, *29*, 9031–9040.
(47) Kim, Y.; Li, W.; Shin, S.; Lee, M. *Acc. Chem. Res.* **2013**, *46*, 2888–2897.
(48) Wilson, C. P.; Webb, S. J. *Chem. Commun.* **2008**, 4007–4009.
(49) Sakai, N.; Mareda, J.; Matile, S. *Acc. Chem. Res.* **2008**, *41*, 1354–1365.
(50) Fyles, T. M. *Chem. Soc. Rev.* **2007**, *36*, 335–347.
(51) Koçer, A.; Walko, M.; Meijberg, W.; Feringa, B. L. *Science* **2005**, *309*, 755–758.
(52) Ghadiri, M. R.; Granja, J. R.; Milligan, R. A.; McRee, D. E.; Khazanovich, N. *Nature* **1993**, *366*, 324–327.
(53) Nakano, A.; Xie, Q.; Mallen, J. V.; Echegoyen, L.; Gokel, G. W. *J. Am. Chem. Soc.* **1990**, *112*, 1287–1289.
(54) Kano, K.; Fendler, J. H. *Biochim. Biophys. Acta* **1978**, *509*, 289–299.
(55) Matile, S.; Sakai, N. The Characterization of Synthetic Ion Channels and Pores. In *Analytical Methods in Supramolecular Chemistry;* Schalley, C. A. Ed.; Wiley-VCH: Weinheim, 2007.
(56) Among Li^{+}, Na^{+} and K^{+}, both channels consisting of **1** and **2** show faster transportation for the smaller cations. On the basis of the Eisenman theory on the ion permeability, this trend suggests that the cation selectivity is mainly determined by the binding energy between cation and the channels, which implies that cation–π interaction at the aromatic portions of **1** and **2** is likely the major driving force for the transportation (Figure S8, Eisenman, G.; Horn, R. *J. Membrane Biol.* **1983**, *76*, 197–225).
(57) Chui, J. K. W.; Fyles, T. M. *Chem. Soc. Rev.* **2012**, *41*, 148–175.
(58) Hille, B. *Ion Channels of Excitable Membrane*, 3rd. ed.; Sinauer Associates: Sunderland, MA, 2001.
(59) Smart, O. S.; Breed, J.; Smith, G. R.; Sansom, M. S. P. *Biophys. J.* **1997**, *72*, 1109–1126.
(60) In fact, we confirmed Me_4N^{+} (ionic diameter: 0.566 nm) was transported by **1** and **2**, while *n*-Bu_4N^{+} (0.830 nm) were transported very inefficiently by either of them probably due to the

insufficient channel sizes (Figure S7, Ue, M. *J. Electrochem. Soc.* **1994**, *141*, 3336–3342).
(61) Sukharev, S. *Biophys. J.* **2002**, *83*, 290–298.
(62) Sukharev, S. I.; Sigurdson, W. J.; Kung, C.; Sachs, F. *J. Gen. Physiol.* **1999**, *113*, 525–539.
(63) Tabata, K. V.; Sato, K.; Ide, T.; Nishizaka, T.; Nakano, A.; Noji, H. *EMBO J.* **2009**, *28*, 3279–3289.

TOC Graphic

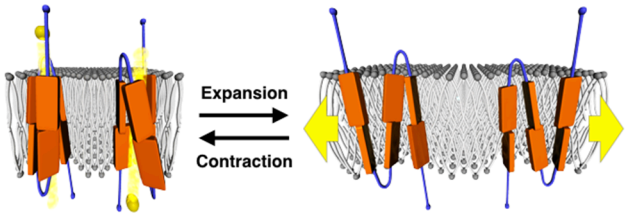

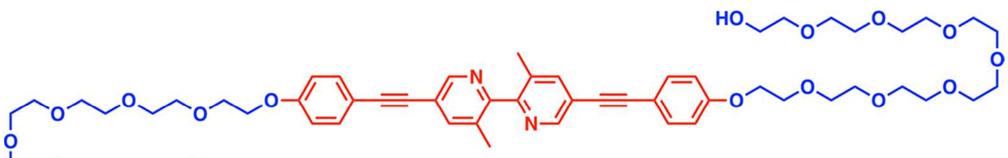

1

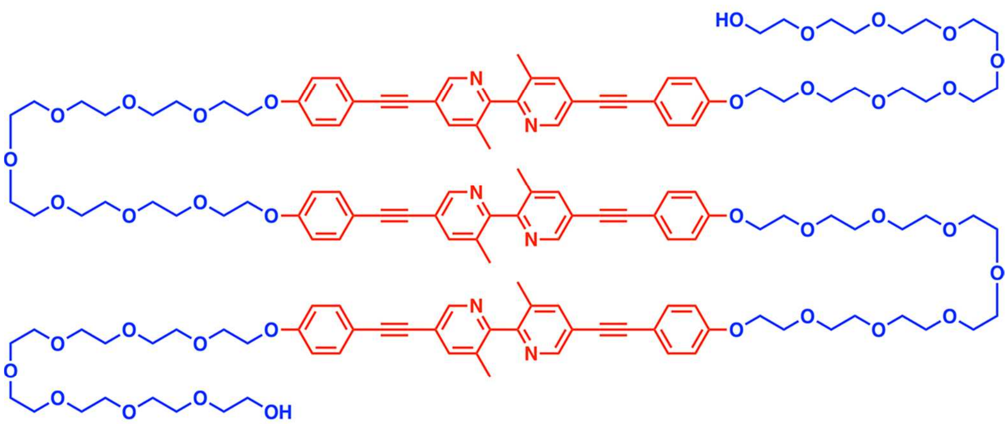

2

Figure 1. Molecular structures of multi-block amphiphiles **1** and **2**.

109x83mm (300 x 300 DPI)

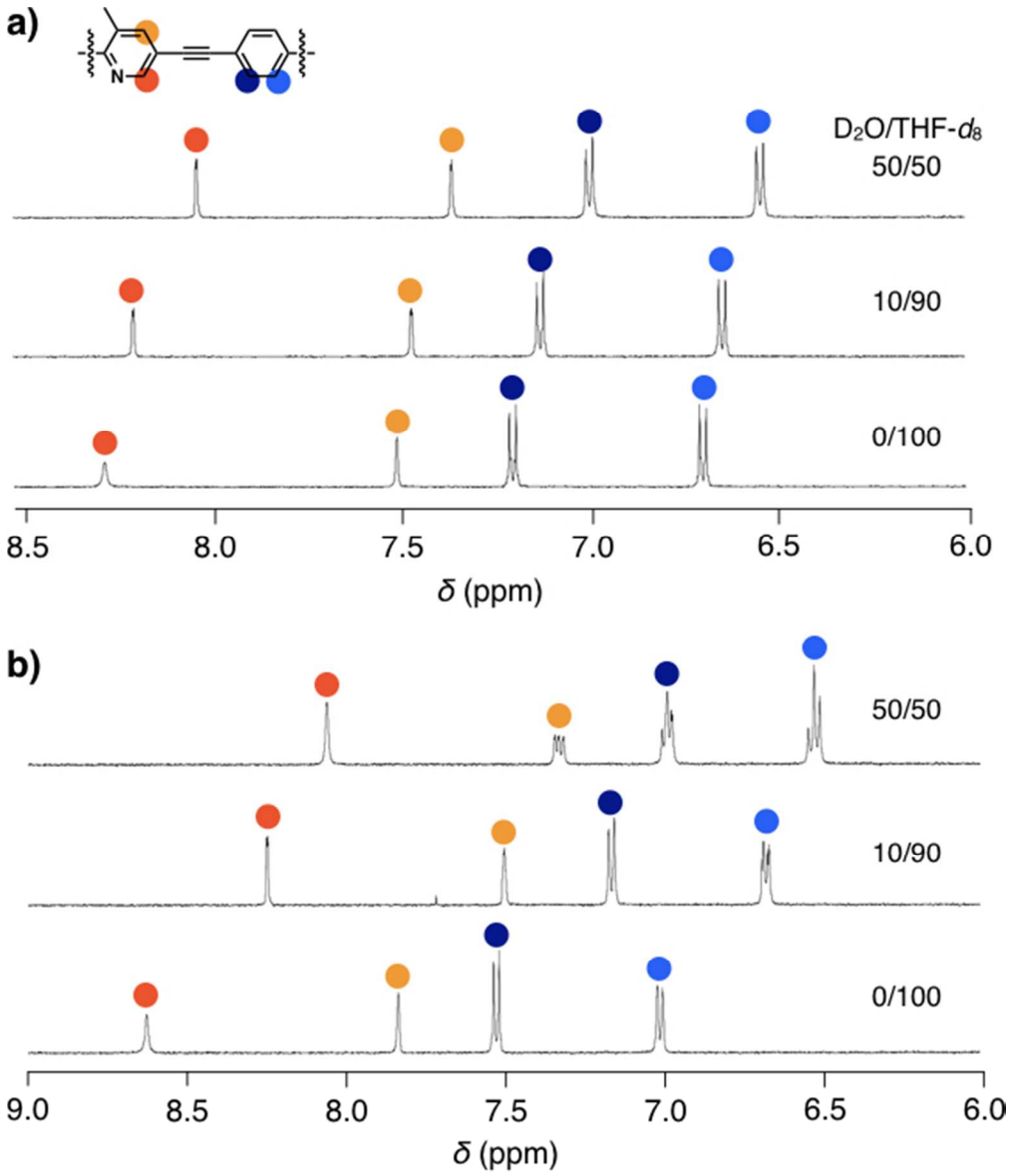

Figure 2. ^{1}H nuclear magnetic resonance spectra of (a) **1** and (b) **2** in the mixtures of D_2O and THF-d8 at various ratios at 25 °C. [**1**] = 3.0 mM and [**2**] = 1.0 mM ([BPBP units] = 3.0 mM for both cases).

227x265mm (72 x 72 DPI)

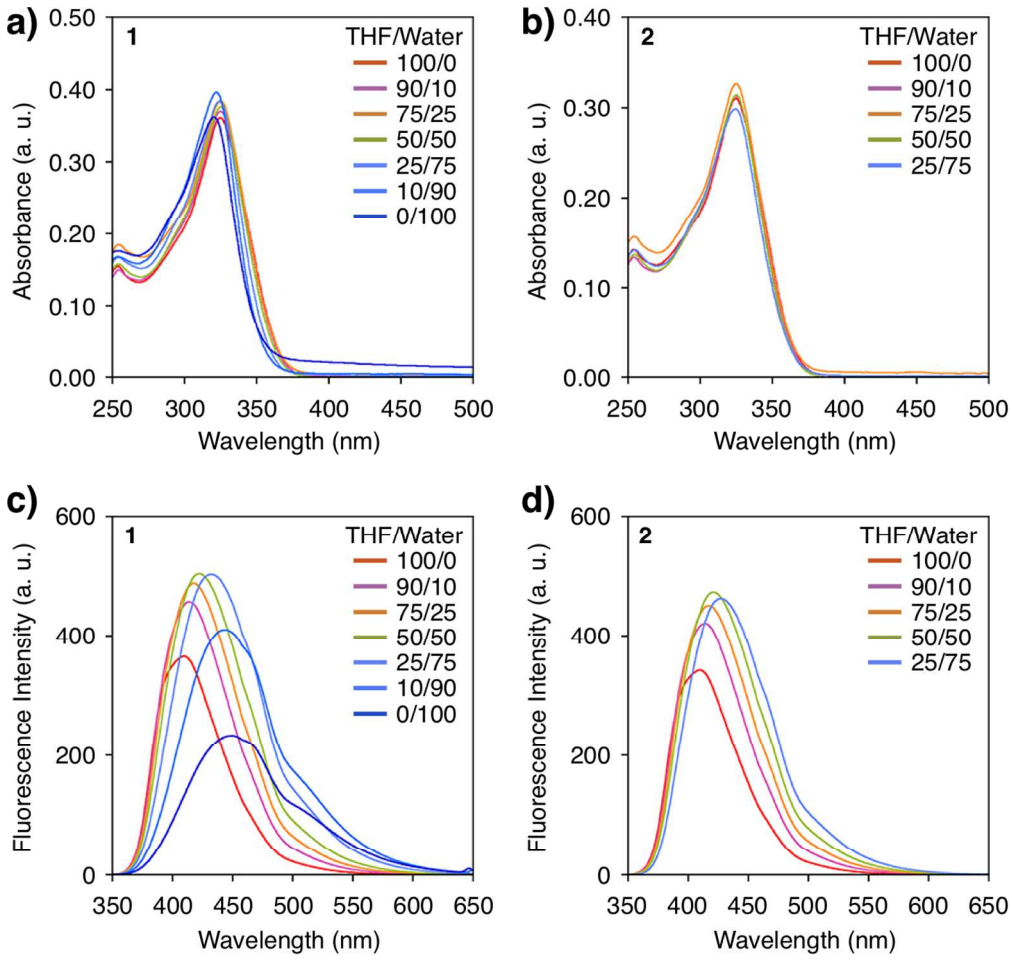

Figure 3. (a,b) Absorption and (c,d) fluorescence spectra of (a,c) **1** and (b,d) **2** in the mixtures of THF and water at 25 °C. The fluorescence spectra were measured upon excitation with 330 nm light for **1** and 328 nm light for **2**, respectively. Optical path length: 1.0 cm. [**1**] = 7.5 μM and [**2**] = 2.5 μM ([BPBP units] = 7.5 μM for both cases).

116x110mm (300 x 300 DPI)

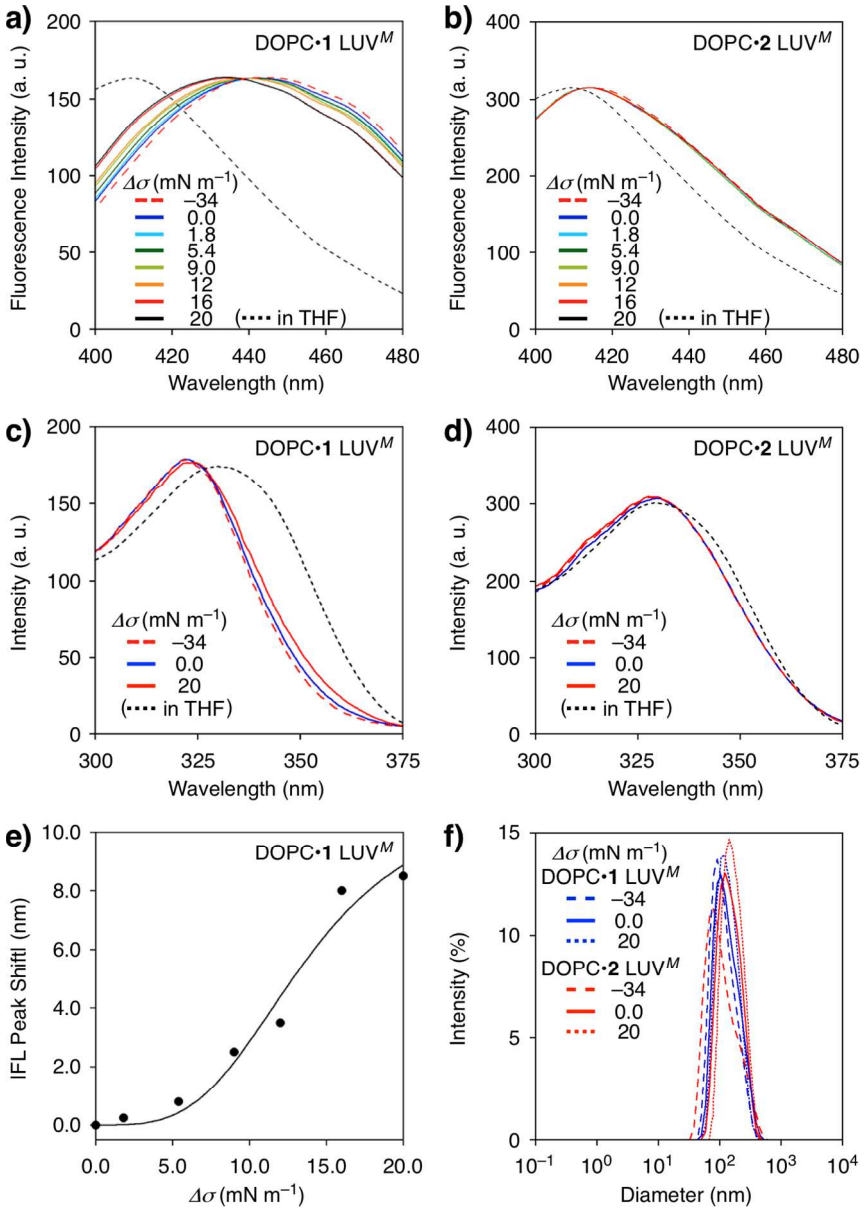

Figure 4. (a,b) Fluorescence and (c,d) excitation spectra of (a,c) DOPC•**1** and (b,d) DOPC•**2** LUV^{M}s in water (solid and dashed lines) under varying membrane tensions and in THF (black dotted lines) at 25 °C. The fluorescence spectra were measured upon excitation with 325 nm light. The excitation spectra were measured monitoring the fluorescence at 440 nm. [**1**]/[DOPC] = 0.050, [**2**]/[DOPC] = 0.017 ([BPBP units] = 10 μM for both cases), [DOPC] = 0.20 mM. The whole spectra (375–600 nm) of (a) and (b) are displayed in the Supporting Figure S5a,b. (e) Absolute values of the fluorescence peak shift of DOPC•1 LUV^M from λ_{FL} = 443 nm at $\Delta\sigma$ = 0 mN m^{-1} in water as a function of the mem-brane tension. The plot was analyzed by curve-fitting with Hill equation (R = 0.9868). (f) Volume-averaged DLS profiles of DOPC•**1** LUV^M (blue) and DOPC•**2** LUV^M (red) in water under tensionless (solid lines) and tensioned (–34 mN m^{-1}: dashed lines, 20 mN m^{-1}: dotted lines) conditions. [**1**]/[DOPC] = 0.050, [**2**]/[DOPC] = 0.017 ([BPBP units] = 10 μM for both cases), [DOPC] = 0.20 mM. Mean hydrodynamic diameters: (DOPC•**1** LUVM) 129 nm at –34 mN m^{-1}, 135 nm at 0 mN m^{-1}, 143 nm at 20 mN m^{-1}, (DOPC•**2** LUVM) 126 nm at –34 mN m^{-1}, 147 nm at 0 mN m^{-1}, 171 nm at 20 mN m^{-1}.

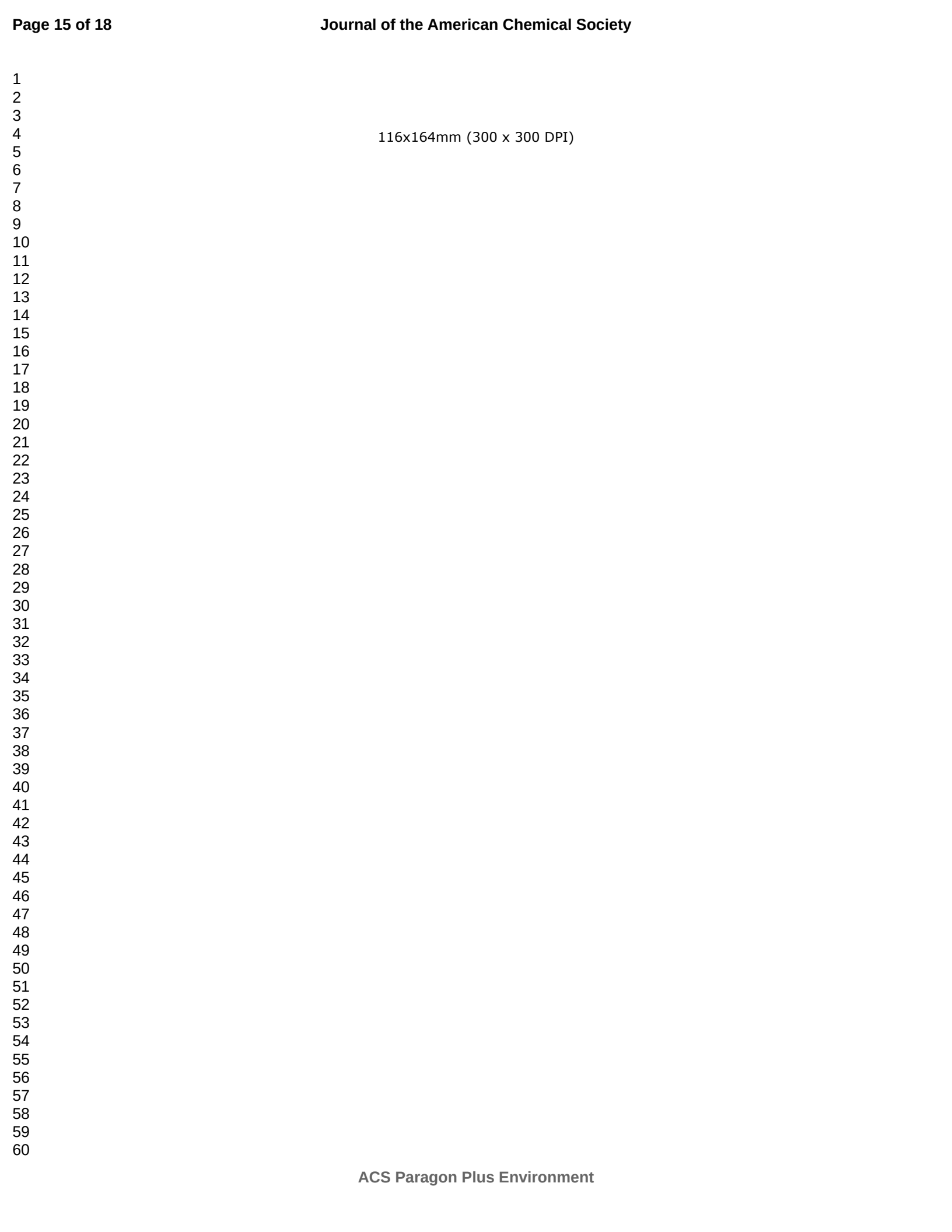
116x164mm (300 x 300 DPI)

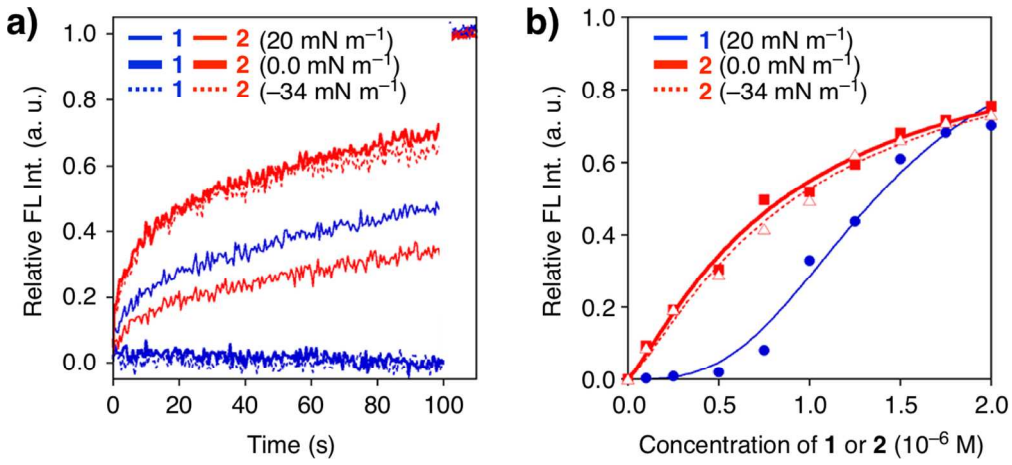

Figure 5. (a) Changes in fluorescence intensity of HPTS en-capsulated in DOPC•**1** and DOPC•**2** LUVMs in HEPES buffer at 20 °C as a function of time after the addition of KOH at 0 sec followed by addition of 1.0 wt% triton X-100 at 100 sec ([DOPC] = 0.20 mM, [**1**] = 1.0 μM, [**2**] = 0.33 μM, [HPTS] = 30 μM, 20 mM HEPES, 50 mM KCl, pH 7.1, excitation at 460 nm, emission at 510 nm). ΔpH = 0.8 (7.1 to 7.9). Tensions added to DOPC•**1** LUV^{M}⊃HPTS (blue lines) and DOPC•**2** LUV^{M}⊃HPTS (red lines): 0 (thick lines), 20 (thin lines) and −34 mN m^{-1} (dotted lines). (b) Plots of relative 510-nm fluo-rescence intensities of HPTS encapsulated in DOPC•**1** and DOPC•**2** LUV^{M}s at 30 s after the addition of KOH in 20 mM HEPES buffer containing 50 mM KCl at 20 °C as a function of concentration of **1** and **2**. Curve-fitting analyses were carried out by the Hill equation (R = 0.993 (DOPC•**1** LUV^{M} at 20 mN m^{-1}), 0.996 (DOPC•**2** LUV^{M} at 0.0 mN m^{-1}), 0.995 (DOPC•**2** LUV^{M} at −34 mN m^{-1})). Colors and line types cor-respond to those in (a).

115x52mm (300 x 300 DPI)

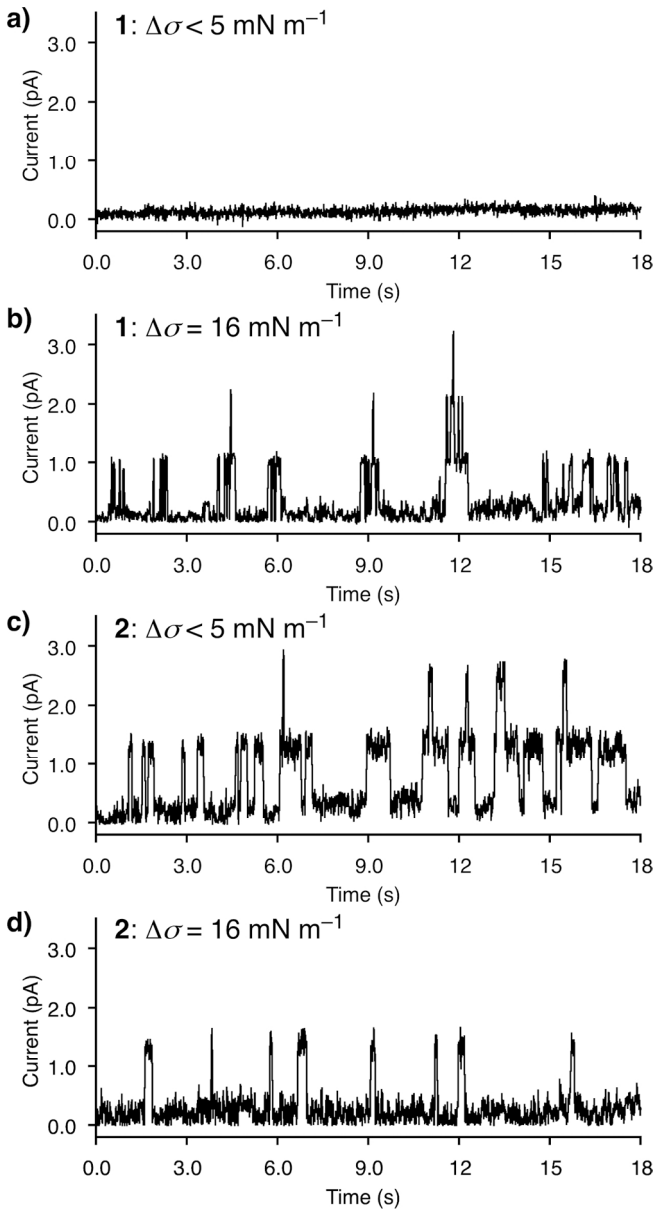

Figure 6. Current traces at the applied voltage of 120 mV of a DOPC BLM containing (a,b) **1** or (c,d) **2** ([**1**]/[DOPC] = 0.010, [**2**]/[DOPC] = 0.0033) in HEPES buffer (20 mM HEPES, 50 mM KCl, 2.0 mM $MgCl_2$, pH 7.5) under (a,c) low tension ($\Delta\sigma$ < 5 mN m^{-1}) or (b,d) increased expanding tension ($\Delta\sigma$ = 16 mN m^{-1}) at 20 °C.

106x197mm (300 x 300 DPI)

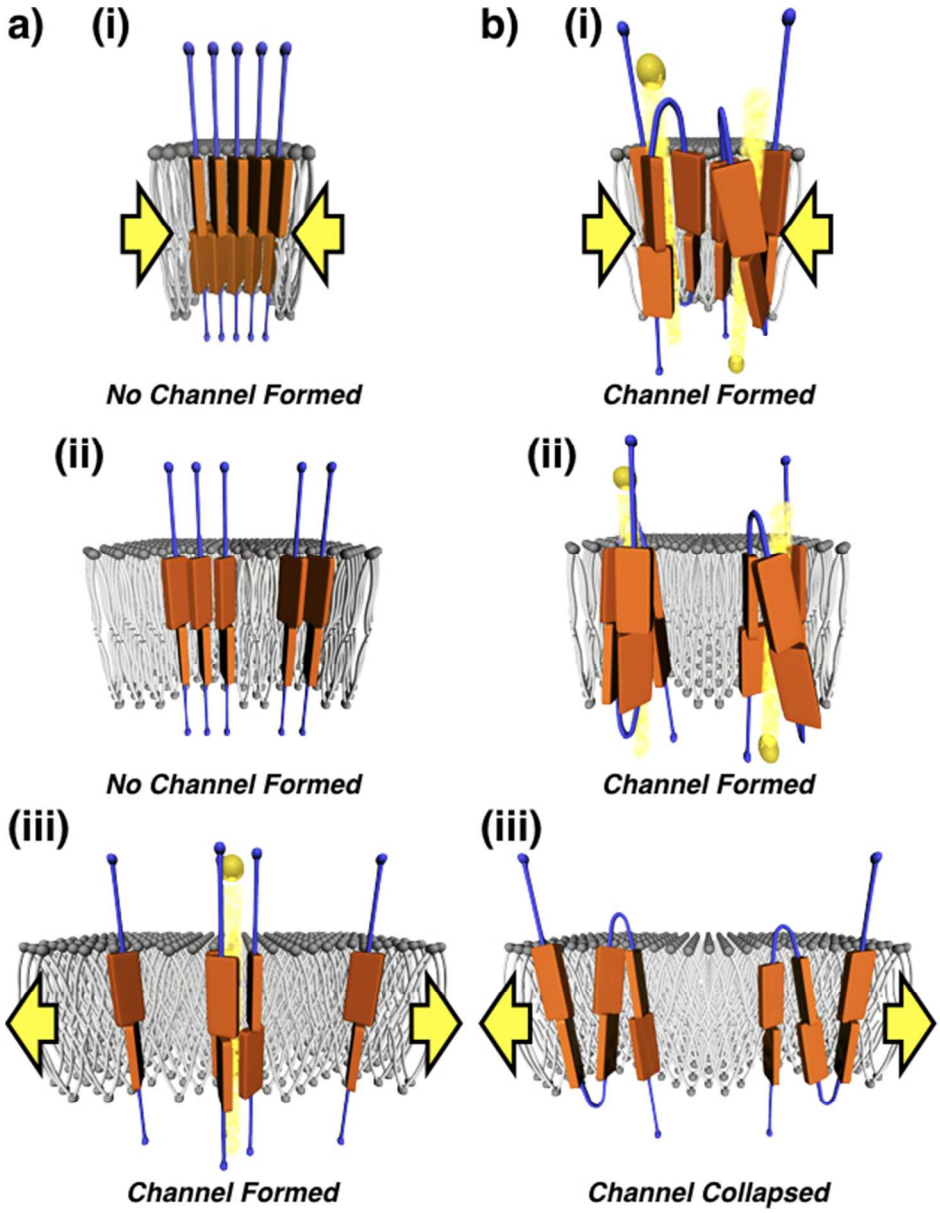

Figure 7. Schematic illustrations displaying the responses of (a) **1** and (b) **2** to (i) membrane contraction and (iii) expansion from (ii) a tensionless condition in a DOPC bilayer. Orange, blue and gray parts denote the hydrophobic and hydrophilic parts in 1 and **2** and DOPC, respectively. Yellow spheres represent a cation. Yellow arrows depict the direction of membrane tension.

220x282mm (72 x 72 DPI)

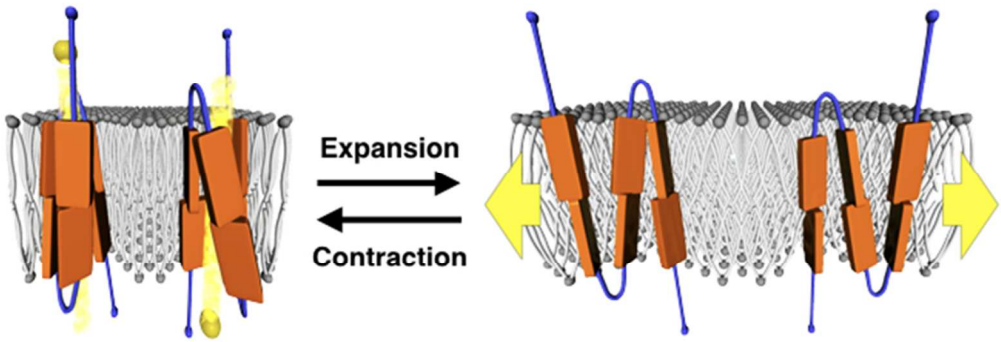

File for TOC.

82x44mm (300 x 300 DPI)